Journal of The Electrochemical Society

MOF-Derived $Co_{1-x}V_xS_y$ Nanosheets as a Highly Efficient Electrocatalyst for Water Splitting

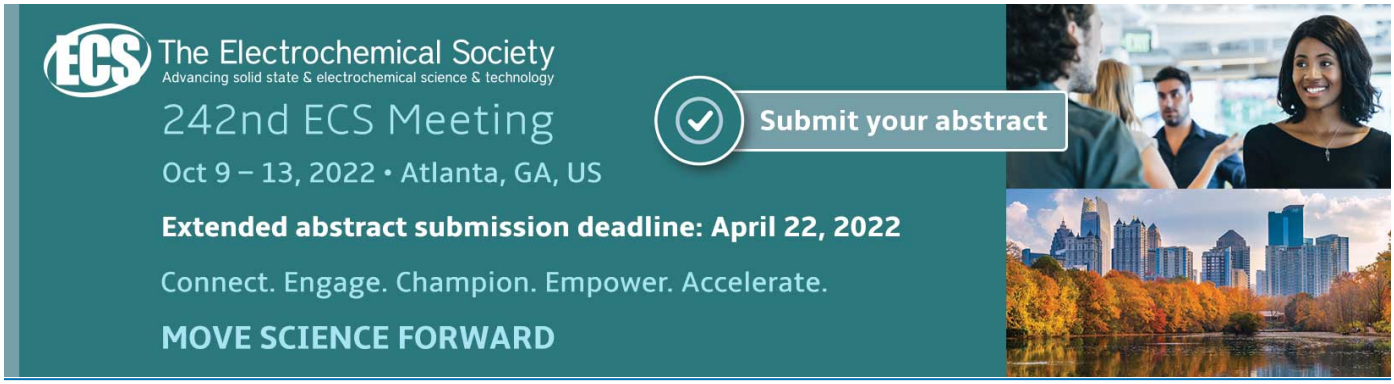

Journal of The Electrochemical Society, 2022 **169** 046507
1945-7111/2022/169(4)/046507/6/$40.00 © 2022 The Electrochemical Society ("ECS"). Published on behalf of ECS by IOP Publishing Limited

MOF-Derived $Co_{1-x}V_xS_y$ Nanosheets as a Highly Efficient Electrocatalyst for Water Splitting

Changtong Lu,[1,2] Jing Yang,[1] Xiaojing Wang,[2] Feng Gao,[1] Xubiao Luo,[3] Xinman Tu,[3] Fengli Qu,[2,z] and Limin Lu[1,z]

[1]*Key Laboratory of Chemical Utilization of Plant Resources of Nanchang, College of Science, Jiangxi Agricultural University, Nanchang 330045, People's Republic of China*
[2]*College of Chemistry and Chemical Engineering, Qufu Normal University, Qufu 273165, Shandong, People's Republic of China*
[3]*Key Laboratory of Jiangxi Province for Persistent Pollutants Control and Resources Recycle, Nanchang Hangkong University, Nanchang 330063, People's Republic of China*

To address issues of global energy sustainability, it is of great practical significance to develop low cost and high efficiency electrocatalysts for the oxygen evolution reaction (OER). In this work, we synthesize amorphous $Co_{1-x}V_xS_y$ nanosheets using $Co_{1-x}V_x$-MOF/NF as a precursor to explore the structural evolution of metal-organic framework (MOF) derivatives during the OER. When tested for OER performance in 1.0 M KOH solution, $Co_{0.9}V_{0.1}S_{0.002}$/NF exhibits the best catalytic activity, with an overpotential of only 194 mV at a current density of 20 mA cm^{-2} and a Tafel slope of 28.4 mV dec^{-1}. We also measured the long-term electrochemical durability of $Co_{0.9}V_{0.1}S_{0.002}$/NF and found that $Co_{0.9}V_{0.1}S_{0.002}$/NF maintains its stability for at least 100 h at a current density of 20 mA cm^{-2}.
 [DOI: 10.1149/1945-7111/ac6394]

Manuscript submitted January 23, 2022; revised manuscript received March 9, 2022. Published April 11, 2022.

Supplementary material for this article is available online

Global energy use has caused a host of adverse environmental and economic consequences.[1,2] The development of clean and renewable energy is an important global goal of the 21st century.[3,4] Hydrogen (H_2) has the potential to be a clean and renewable energy carrier, but currently, the majority of H_2 is produced from fossile fuels via the steam reforming of CH_4. However, electrochemical water splitting is promising way to produce H_2 in a clean manner because the electricity needed from electrolysis can originate from clean and renewable energy sources such as solar and wind.[5–8]

The OER from H_2O involves four-electron transfer steps, and the complications arising from these multiple electron transfer steps frequently cause sluggish reaction kinetics and high overpotential.[9,10] Therefore, it is important to design new electrocatalysts that facilitate the OER at low overpotentials. In recent years, IrO_2 and RuO_2 have become the most commercially valuable OER catalysts.[11–15] However, due to the scarcity and instability of these precious metals, their application in industrial production is still in its infancy.[16] Therefore, it remains a grand challenge to develop efficient, cheap, stable and abundant alternative electrocatalysts for electrochemical water splitting.[17,18]

Metal-organic frameworks (MOFs) with self-supporting structures can improve OER performance by providing more active sites and adjusting electron transfer dynamics.[19–24] Unfortunately, most MOFs show poor intrinsic electric conductivity and electrocatalytic activity.[25–28] The direct use of MOFs as an effective water splitting catalyst is therefore not currently effective. To further improve OER performance, it is important to optimize the properties of MOFs. There are several ways to improve the performance of MOFs. First, transition metal sulfides can be used because of their excellent electrochemical properties and electroconductivities.[29–32] Therefore, the use of MOFs as templates to synthesize sulfides has been widely used in water splitting;[33] s, multi-metallic MOFs are conducive to the formation of materials with a large number of active sites, adjustable electronic configurations, and improved electrical conductivity. These beneficial properties work in tandem to yield enhanced electrocatalysts for a variety of electrochemical reactions.[34–37] Inspired by these stratrgies, we hypothesized that the multi-step optimization of MOFs may greatly improve the performance of water-splitting catalysts. Current studies have shown that high-valent V is beneficial to the OER and can readily form in a variety of synthesis processes.[38,39] In addition, V has a variety of composition forms, rich oxidation states and coordination polyhedra, which provides great feasibility for controlling its structural properties and related functions.[40,41] To complement the beneficial properties of V, Co-MOF was chosen as the optimized precursor because Co is active OER material.[42] Therefore, we speculate that the use of high valent V to replace part of Co to construct CoV-MOF followed by sulfurization, will optimize the electronic structure of the active site, thus improving water splitting performance.

In the present study, MOF-derived $Co_{1-x}V_xS_y$ nanosheets array grown on Ni foam ($Co_{1-x}V_xS_y$/NF) were successfully synthesized via a two-step hydrothermal process (Scheme 1). We first optimized the ratio of Co and V, and the products obtained were $Co_{0.95}V_{0.05}$-MOF/NF, $Co_{0.9}V_{0.1}$-MOF/NF, $Co_{0.8}V_{0.2}$-MOF/NF, and $Co_{0.7}V_{0.3}$-MOF/NF, respectively. Next, we selected the best performance of $Co_{0.9}V_{0.1}$-MOF/NF for further sulfurization. To further optimize the performance of the catalyst, $Co_{0.9}V_{0.1}S_{0.001}$/NF, $Co_{0.9}V_{0.1}S_{0.002}$/NF, $Co_{0.9}V_{0.1}S_{0.003}$/NF, and $Co_{0.9}V_{0.1}S_{0.004}$/NF were obtained by adjusting the concentration of thioacetamide (TAA) in the solution. After the introduction of electronegative S, S atoms partially replaced O atoms in $Co_{0.9}V_{0.1}$-MOF/NF. Due to the difference in electronegativity and atomic radii of the two elements, the original long-range lattice structure is destroyed, forming an amorphous structure. When tested for OER performance in 1.0 M KOH solution, this $Co_{0.9}V_{0.1}S_{0.002}$/NF exhibits the best catalytic activity, with an overpotential of only 194 mV at a current density of 20 mA cm^{-2} and with a Tafel slope of 28.4 mV dec^{-1}. We also measured the long-term electrochemical durability of $Co_{0.9}V_{0.1}S_{0.002}$/NF and found that $Co_{0.9}V_{0.1}S_{0.002}$ is stable for at least 100 h at a current density of 20 mA cm^{-2}. In addition, we also discuss the structural evolution of the MOF derivatives during the OER process.

Experimental

Chemicals.—All the chemicals were of analytical grade, purchased from Aladdin Reagent Co. Ltd, and were used without further purification. Nickel foam was obtained from Tianjin Aiwexin Chemical Technology Co.Ltd, with a thickness of 1 mm. The Ni foam was first cut into pieces at a size of 2 cm × 4 cm. Then the NF was successively sonicated in 15% HCl and water, followed by drying at 60 °C.

[z]E-mail: fengliquhn@hotmail.com; lulimin816@hotmail.com

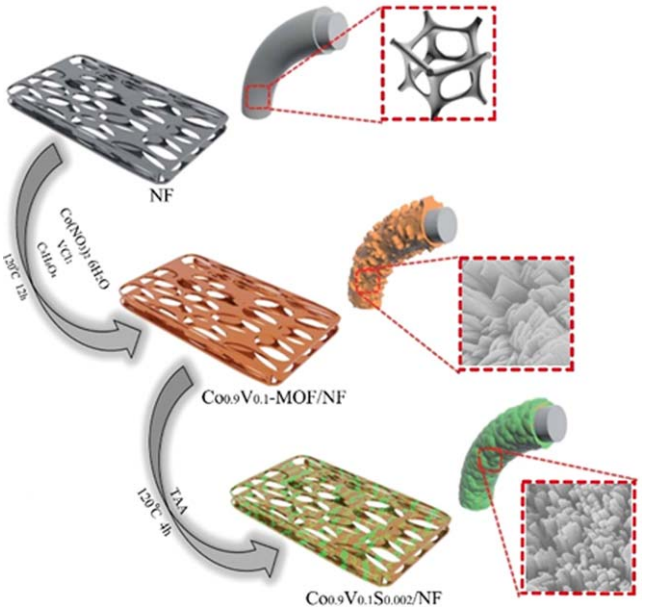

Scheme 1. Schematic illustration of the fabrication process for $Co_{0.9}V_{0.1}S_{0.002}$/NF.

Synthesis of $Co_{0.9}V_{0.1}$-MOF/NF.—$Co(NO_3)_2{\cdot}6H_2O$ (4.725 mmol), VCl_3 (0.525 mmol) and H_2BDC (3.8 mmol) were dissolved in 70 ml of DMF, 5 ml of ethanol, and 5 ml of ultrapure water. The mixture was then magnetically stirred for 30 min to acquire a homogeneous aqueous solution, which was moved to a high-pressure reaction kettle. The NF was inserted into the above-mentioned reaction kettle and reacted at 120 °C for 12 h. After that, the reactor was cooled to 25 °C. $Co_{0.9}V_{0.1}$-MOF/NF was taken out, rinsed with ultrapure water and ethanol, and dried at 70 °C for 3 h. $Co_{0.95}V_{0.05}$-MOF/NF, $Co_{0.8}V_{0.1}$-MOF/NF, and $Co_{0.7}V_{0.3}$-MOF/NF were synthesized by the above method.

Synthesis of $Co_{0.9}V_{0.1}S_{0.002}$/NF.—0.002 mol TAA was dispersed in 80 ml of ultrapure water, and then the aqueous solution was poured into a Teflon-lined stainless-steel autoclave. $Co_{0.9}V_{0.1}$-MOF/NF was placed in the reactor and kept at 120 °C for 4 h to obtain $Co_{0.9}V_{0.1}S_{0.002}$/NF nanosheets. The reactor was then cooled to 25 °C. Subsequently, $Co_{0.9}V_{0.1}S_{0.002}$/NF was taken out of the reactor and rinsed with ultrapure water and ethanol for 3 times, and dried at 70 °C for 3 h. $Co_{0.9}V_{0.1}S_{0.001}$/NF, $Co_{0.9}V_{0.1}S_{0.003}$/NF, and $Co_{0.9}V_{0.1}S_{0.004}$/NF were synthesized by the above method.

Physical characterization.—Powder X-ray diffraction (XRD) patterns were performed using a RigakuD/MAX 2550 diffractometer with Cu Kα radiation ($\lambda = 1.5418$ Å). Scanning electron microscope (SEM) measurements were recorded on a XL30 ESEM FEG scanning electron microscope at an accelerating voltage of 20 kV. The structures of the samples were determined by Transmission electron microscopy (TEM) images on a HITACHI H-8100 electron microscopy (Hitachi, Tokyo, Japan) operated at 200 kV. Xray photoelectron spectroscopy (XPS) data of the samples was collected on an ESCALABMK II X-ray photoelectron spectrometer using Mg as the exciting source.

Electrochemical measurements.—Electrochemical measurements were carried out in a standard three-electrode system controlled by using a CHI 760D electrochemical workstation (Chenhua Company, Shanghai) in an electrolyte solution of 1.0 M KOH. $Co_{0.9}V_{0.1}S_{0.002}$/NF with dimensions of 0.5 cm × 0.5 cm were used directly as working electrodes. Graphite plates, and a Hg/HgO electrode were used as the counter and reference electrodes, respectively. Each working electrode was activated by cyclic voltammetry (CV) with a scan rate of 50 mV s^{-1} until a stable CV curve was obtained. After that, the polarization curve was measured with linear sweep voltammetry (LSV) at room temperature with a

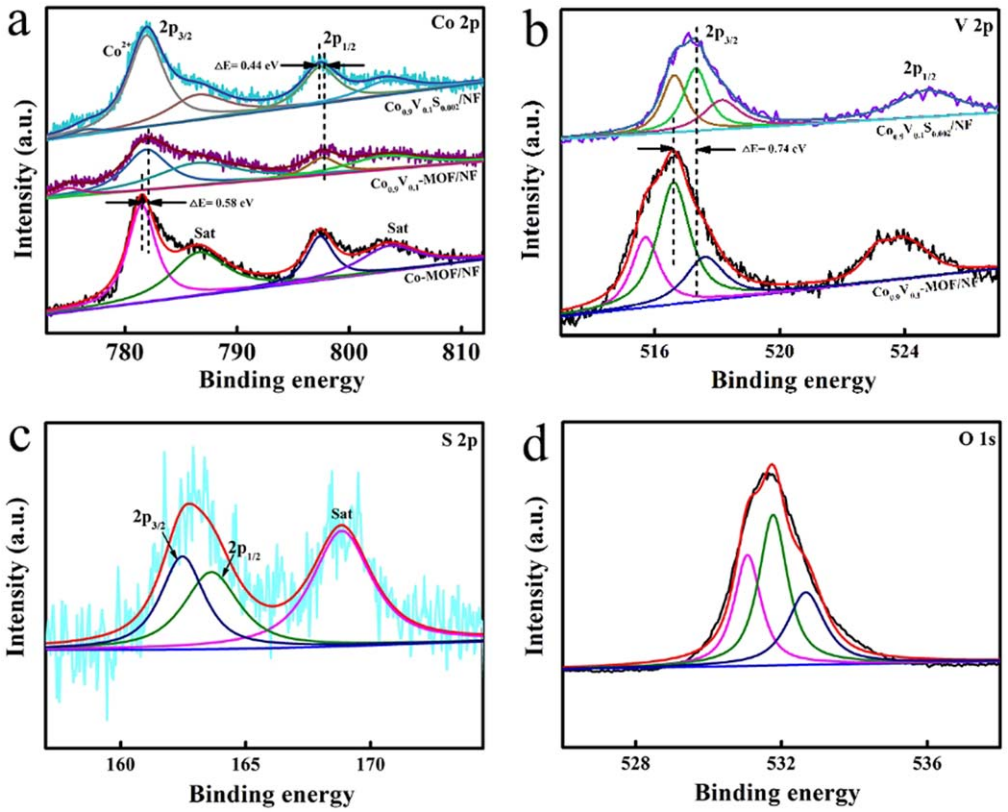

Figure 1. XPS of Co-MOF/NF, $Co_{0.9}V_{0.1}$-MOF/NF, and $Co_{0.9}V_{0.1}S_{0.002}$/NF. High-resolution spectra of (a) Co, (b) V, (c) S, and (d) O.

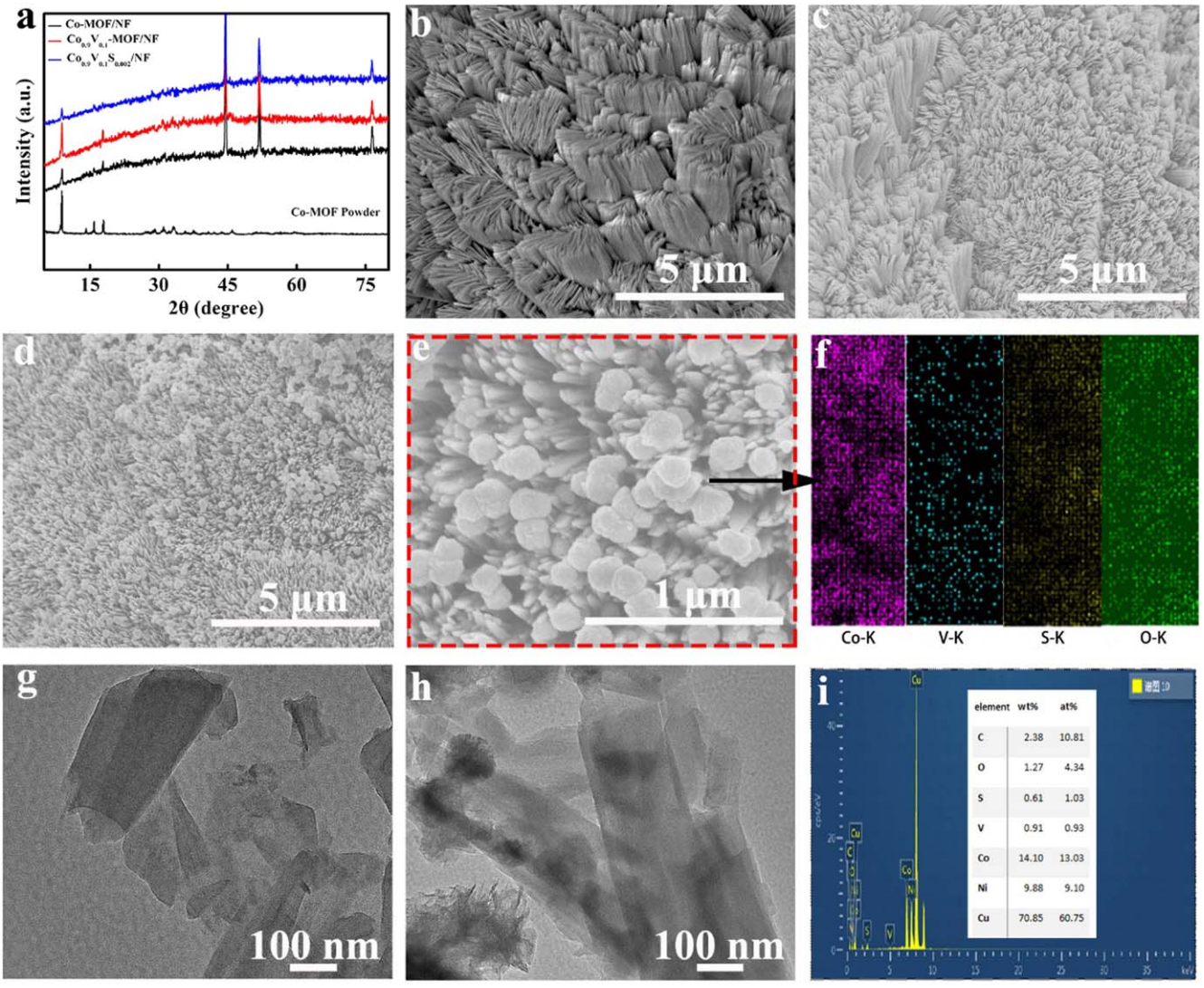

Figure 2. (a) XRD patterns of the $Co_{0.9}V_{0.1}S_{0.002}$/NF, $Co_{0.9}V_{0.1}$-MOF/NF, and Co-MOF/NF. SEM images of (b) Co-MOF/NF, (c) $Co_{0.9}V_{0.1}$-MOF /NF, (d) $Co_{0.9}V_{0.1}S_{0.002}$/NF, and (e) $Co_{0.9}V_{0.1}S_{0.002}$/NF. (f) EDX elemental mapping images of Co, V, S, and O for $Co_{0.9}V_{0.1}S_{0.002}$/NF. TEM images of (g) $Co_{0.9}V_{0.1}$-MOF and (h) $Co_{0.9}V0.1S_{0.002}$/NF. (h) Elemental analysis of selected regions by TEM-EDX.

scan rate of 2 mV s^{-1}. All the potentials measured in this study were converted to the reversible hydrogen electrode (RHE) scale according to the Nernst equation: E (RHE) = E (Hg/HgO) + (0.098 + 0.059*pH) V. Overpotential values were calculated as follows: $\eta = E_{vs.RHE} - 1.23$ V. Electrochemical impedance spectroscopy (EIS) at 0.28 V (vs RHE) data were collected with a frequency range from 0.1 Hz to 100 KHz and an alternating voltage of 5 mV. The electrochemical surface area (ECSA) was investigated by double-layer capacitance (C_{dl}) in the potential range from 1.02 V to 1.12 V vs RHE. iR correction of LSVs was performed to avoid the influence of electrolyte ohmic resistance (R_s). The corrected potential was obtained by using:

$$E_{corrected} = E_{measured} - iR_s$$

Where, i is the measured current density and R_s is obtained from EIS testing. To reflect the intrinsic behavior of the catalysts, all experimental data are corrected with ohmic potential drop (IR) losses resulting from the solution resistance.

Results and Discussion

Structure characterization.—First, the valence states and elemental composition of the $Co_{0.9}V_{0.1}S_{0.002}$/NF were analyzed by X-ray photoelectron spectroscopy (XPS). The high-resolution Co 2p spectrum of $Co_{0.9}V_{0.1}S_{0.002}$/NF is shown in Fig. 1a. Typically, the two peaks at 782.1 eV and 797.4 eV are ascribed to Co (II) $2p_{3/2}$ and Co (II) $2p_{1/2}$ respectively, confirming the presence of Co^{2+}. The peaks at 787.1 eV and 803.5 eV are due to satellites of Co (marked as Sat).[43] Compared with Co-MOF/NF, the Co $2p_{3/2}$ peak positions of $Co_{0.9}V_{0.1}$-MOF/NF shift to higher binding energies, which also indicates that there are electronic interactions between the two metals. Interestingly, compared with the Co $2p_{1/2}$ peak of $Co_{0.9}V_{0.1}$-MOF/NF and $Co_{0.9}V_{0.1}S_{0.002}$/NF, the peak positions of $Co_{0.9}V_{0.1}S_{0.002}$/NF shift to lower binding energies. Therefore, we hypothesize that the successful introduction of V and S is not simply due to physical adsorption, but that it results in an optimization of the electronic structure of Co^{2+}. The high-resolution V 2p spectrum of $Co_{0.9}V_{0.1}S_{0.002}$/NF is shown in Fig. 1b. The peaks at 515.7 eV, 516.7 eV and 517.6 eV are attributed to V^{3+}, V^{4+} and V^{5+}, respectively.[44,45] Similarly, the successful introduction of S also adjusts the electronic structure of V, which makes the V $2p_{3/2}$ transition shift towards a higher binding energy. Figure 1c displays the S 2p spectrum. The peaks at 162.5 eV and 163.6 eV are ascribed to the metal-S bond.[46] The peak at 168.8 eV can be attributed to the S species with a high oxidation state.[47,48] In the O 1 s spectrum, the peaks at 531.2 eV, 532.1 eV, and 532.9 eV are attributed to V-O bond, O-H bond, and adventitious water, respectively (Fig. 1d).[49]

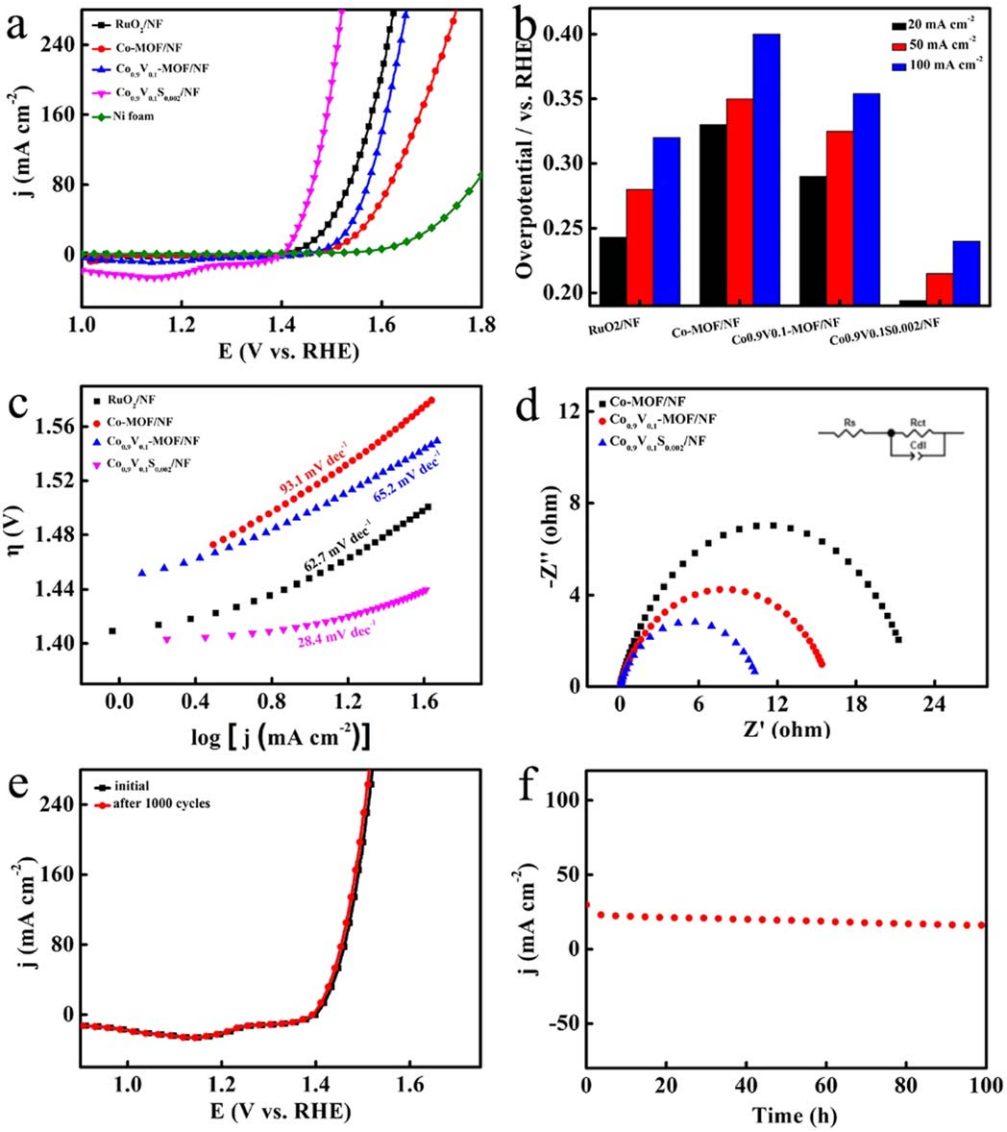

Figure 3. (a) LSV curves for Ni foam, RuO_2/NF, Co-MOF/NF, $Co_{0.9}V_{0.1}$-MOF/NF and $Co_{0.9}V_{0.1}S_{0.002}$/NF at a scan rate of 2 mV s^{-1}. (b) Overpotential of RuO_2/NF, Co-MOF/NF, $Co_{0.9}V_{0.1}$-MOF/NF and $Co_{0.9}V_{0.1}S_{0.002}$/NF at 20 mA cm^{-2}, 50 mA cm^{-2} and 100 mA cm^{-2}, respectively. (c) Tafel plots of RuO_2/NF, Co-MOF/NF, $Co_{0.9}V_{0.1}$-MOF/NF and $Co_{0.9}V_{0.1}S_{0.002}$/NF. (d) Nyquist plots of Co-MOF/NF, $Co_{0.9}V_{0.1}$-MOF/NF and $Co_{0.9}V_{0.1}S_{0.002}$/NF recorded in 1.0 M KOH solution. (e) LSV curves for $Co_{0.9}V_{0.1}S_{0.002}$/NF before and after 1000 cycles. (f) Long-time stability test of the $Co_{0.9}V_{0.1}S_{0.002}$/NF at a constant current density of 20 mA cm^{-2} for 100 h.

The composition was also analyzed by X-ray powder diffraction (XRD). XRD patterns of Co-MOF/NF, $Co_{0.9}V_{0.1}$-MOF/NF, and $Co_{0.9}V_{0.1}S_{0.002}$/NF are shown in Fig. 2a. The XRD patterns of Co-MOF/NF are consistent with the results reported in previous literature[50] and the other peaks at 44.5°, 51.8° and 76.4° are indexed to the (111), (200), and (220) planes of Ni foam (JCPDS no. 04–0850), respectively. Because the crystallinity of V-based oxide is very low,[11,51] there is no significant change in XRD spectrum after the introduction of V into Co-MOF. With the introduction of electronegative sulfur, the diffraction peak of $Co_{0.9}V_{0.1}S_{0.002}$/NF still maintains the original MOFs structure, but the diffraction peak becomes weaker.

In addition, we also demonstrated the successful synthesis of $Co_{0.9}V_{0.1}$-MOF/NF by Fourier transform infrared spectroscopy (FT-IR) (Fig. S1). Characteristic para-aromatic C-H stretching vibration bands occur at 1501 cm^{-1}, 1146 cm^{-1}, 1101 cm^{-1}, 1017 cm^{-1}, 812 cm^{-1}, and 748 cm^{-1}. In addition, the peak value at 649 cm^{-1} is attributed to the Co-O or V-O bond, indicating the formation of metal oxygen bond between the Co or V atom and the terephthalate carboxyl group.

In Fig. 2b, Co-MOF/NF scanning electron microscopy (SEM) images demonstrate that Co-MOF/NF consists of an array of nanosheets. After the introduction of V, $Co_{0.9}V_{0.1}$-MOF/NF forms a smaller nanosheets structure with larger pores, which is conducive to the passage of electrolyte solution (Fig. 2c). After the introduction of S, $Co_{0.9}V_{0.1}S_{0.002}$/NF still retains the properties of nanosheets, but the roughness of the nanosheets increase (Figs. 2d, 2e). Therefore, the introduction of V and S not only adjusts the morphology of the catalyst, but also provides more reaction sites and improves OER performance. The energy-dispersive X-ray (EDX) elemental mapping images for $Co_{0.9}V_{0.1}S_{0.002}$/NF verify the uniform distribution of Co, V, S, and O elements (Fig. 2f). Transmission electron microscopy (TEM) images of $Co_{0.9}V_{0.1}$-MOF/NF and $Co_{0.9}V_{0.1}S_{0.002}$/NF further confirm the morphology of the nanosheets (Figs. 2g and 2h). The EDX elemental mapping images for $Co_{0.9}V_{0.1}S_{0.002}$/NF verify the uniform distribution of Co, V, and S elements (Fig. 2i).

OER Performance.—The electrochemical OER activities of the as-prepared samples were tested using a typical three-electrode system in a 1.0 M KOH solution at a scan rate of 2 mV s^{-1}.

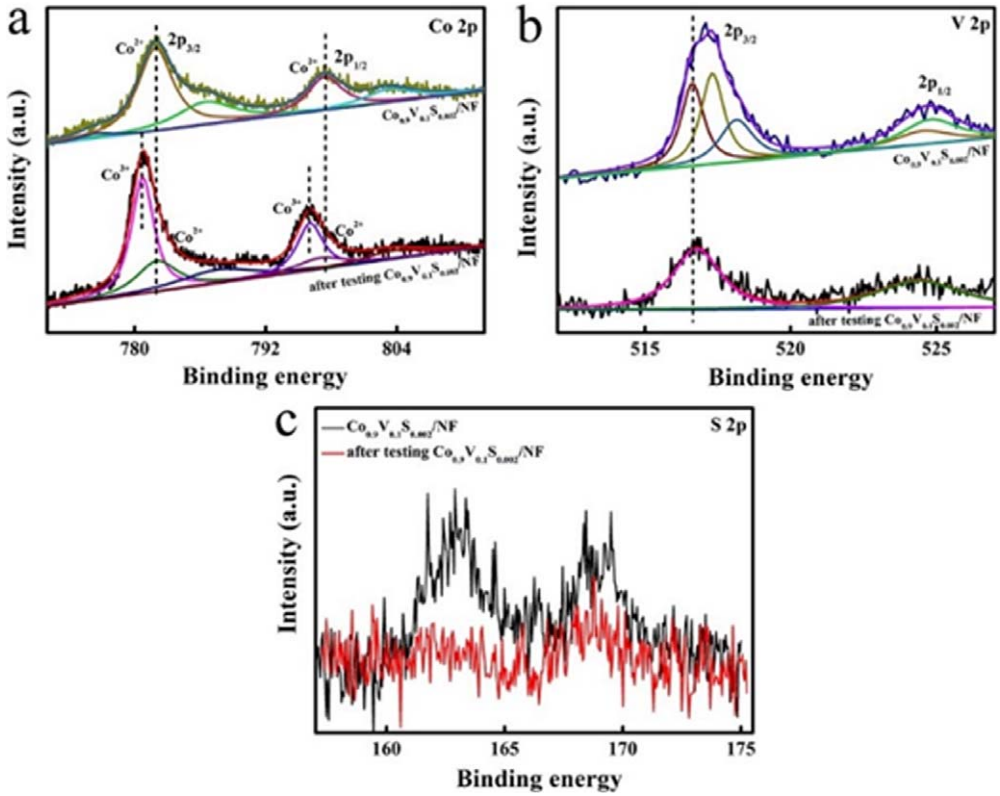

Figure 4. XPS of $Co_{0.9}V_{0.1}S_{0.002}$/NF after testing $Co_{0.9}V_{0.1}S_{0.002}$/NF. High-resolution spectra of (a) Co, (b) V, and (c) S.

The OER performances of Ni foam, RuO_2/NF, Co-MOF/NF, $Co_{0.9}V_{0.1}$-MOF/NF, and $Co_{0.9}V_{0.1}S_{0.002}$/NF were measured under the same conditions. To yield the best catalyst, we first optimized the ratio of Co and V in $Co_{1-x}V_x$-MOF/NF, among which $Co_{0.9}V_{0.1}$-MOF/NF has the best performance (Figs. S2a and S2b). Next, we chose $Co_{0.9}V_{0.1}$-MOF/NF for further sulfurization, and continuously adjusted the content of S during the sulfurization process to obtain $Co_{0.9}V_{0.1}S_{0.002}$/NF nanosheets with the best OER performance (Fig. S2c and S2d). In Fig. 3a, the catalyst $Co_{0.9}V_{0.1}S_{0.002}$/NF exhibits first-rate OER activity, with low overpotentials of 194 mV, 215 mV, and 240 mV, respectively, to reach current density of 20, 50, and 100 mA cm^{-2}, respectively, which is better than those of the RuO_2/NF (243 mV, 280 mV and 320 mV, respectively), Co-MOF/NF (330 mV, 350 mV and 400 mV, respectively), and $Co_{0.9}V_{0.1}$-MOF/NF (290 mV, 325 mV and 354 mV, respectively). The reduction peaks of $Co_{0.9}V_{0.1}S_{0.002}$/NF at 1.2 V and 1.3 V shown in Fig. 3a are attributed to the conversion of Ni^{3+} to Ni^{2+} (Ni ions originate from the Ni foam) and Co^{3+} to Co^{2+}, respectively.[44,49] In addition, the performance of $Co_{0.9}V_{0.1}S_{0.002}$/NF in alkaline medium is superior to that of other non-noble metal OER catalysts (Table SI). The reaction kinetics of OER can be quantified using the Tafel equation ($\eta = b \log j + a$), where b is Tafel slope and j is current density). In Fig. 3c, we calculated the Tafel slope of RuO_2/NF, Co-MOF/NF, $Co_{0.9}V_{0.1}$-MOF/NF, and $Co_{0.9}V_{0.1}S_{0.002}$/NF, and the Tafel values are 62.7 mV dec^{-1}, 93.1 mV dec^{-1}, 62.2 mV dec^{-1}, and 28.4 mV dec^{-1}, respectively, indicating the rapid OER catalytic kinetics of $Co_{0.9}V_{0.1}S_{0.002}$/NF. ECSA is an important parameter to measure the real electrocatalytic activity of electrocatalysts. Therefore, we use double-layer capacitance (C_{dl}) to calculate the size of the ECSA, which further clarifies the reason for the excellent performance of $Co_{0.9}V_{0.1}S_{0.002}$/NF nanosheets. The ECSA can be converted from the C_{dl} by the equation: ECSA = C_{dl}/C_s, where C_s representing the specific capacitance is 0.04 mF cm^{-2}.[12,52] The C_{dl} values for Co-MOF/NF, $Co_{0.9}V_{0.1}$-MOF/NF, and $Co_{0.9}V_{0.1}S_{0.002}$/NF are calculated by means of the cyclic voltammograms (CVs) under different scan rates (Fig. S3a, S3b and S3c). In Fig. S3d, it is found that the C_{dl} of $Co_{0.9}V_{0.1}S_{0.002}$/NF (4.1 mF cm^{-2}) is much greater than those of $Co_{0.9}V_{0.1}$-MOF/NF (2.2 mF cm^{-2}) and Co-MOF/NF (1.4 mF cm^{-2}). Therefore, $Co_{0.9}V_{0.1}S_{0.002}$/NF has a larger ECSA of 102.5 cm^{-2} compared to $Co_{0.9}V_{0.1}$-MOF/NF (ECSA = 55 cm^{-2}) and Co-MOF/NF (ECSA = 35 cm^{-2}), indicating that $Co_{0.9}V_{0.1}S_{0.002}$/NF has stronger anion exchange capacity with electrolyte solution, which is also the reason why $Co_{0.9}V_{0.1}S_{0.002}$/NF has excellent OER performance. Nyquist diagrams show that $Co_{0.9}V_{0.1}S_{0.002}$/NF has a faster charge transfer rate (Fig. 3d), which may be due to the fact that $Co_{0.9}V_{0.1}S_{0.002}$/NF has a larger ECSA and good conductivity. On the other hand, we also calculated the turnover frequency (TOF) of the various catalysts to further investigate the intrinsic activity. As presented in Fig. S4, the calculated TOF value for $Co_{0.9}V_{0.1}S_{0.002}$/NF is 0.21 mol O_2 s^{-1} at an overpotential of 400 mV. Durability is an indispensable parameter to assess the performance of catalysts. In addition, compared with the initial performance, the LSV curve after 1,000 cycles did not deteriorate significantly (Fig. 3e), indicating that $Co_{0.9}V_{0.1}S_{0.002}$/NF has good durability. We also measured the long-term electrochemical durability of $Co_{0.9}V_{0.1}S_{0.002}$/NF and found that $Co_{0.9}V_{0.1}S_{0.002}$/NF can maintain stability for at least 100 h at a current density of 20 mA cm^{-2} (Fig. 3f). The excellent and stable catalytic performance of $Co_{0.9}V_{0.1}S_{0.002}$/NF can be attributed to the following two considerations. First, the introduction of V and S optimized the intrinsic morphology of the catalyst and the electronic structure of the active center. Second, during the OER, the catalyst itself was self-reconstituted, and cobalt vanadium sulfide was transformed into cobalt vanadium sulfide oxide and cobalt vanadium oxide, which are known to be highly durable catalysts for OER.[1,38]

The actual active site of metal nanomaterials in the oxygen evolution reaction comes from the metal oxide/hydroxide formed on the surface.[53] Therefore, we speculate that necessary changes may occur to $Co_{0.9}V_{0.1}S_{0.002}$/NF nanosheets during the OER, We carried out various characterization of the composition and morphology changes of the catalysts before and after the reaction. As shown in Figs. S5a and S5b, high resolution transmission electron microscopy (HRTEM) images and selected area electron diffraction (SAED)

confirm that $Co_{0.9}V_{0.1}S_{0.002}$/NF is amorphous. We hypothesize that after the electronegative sulfur is incorporated, S atoms partially substitute O atoms of $Co_{0.9}V_{0.1}$-MOF/NF. Due to the difference in electronegativity and atomic radius of the two elements, the original long-range lattice structure is destroyed, resulting in the formation of an amorphous structure.[54,55] Interestingly, after the OER test, although the lamellate structure of $Co_{0.9}V_{0.1}S_{0.002}$/NF is retained (Fig. S5c), the amorphous structure on the surface of the nanosheets changes to a crystalline structure. The measured lattice fringe spacing of 0.244 nm can be ascribed to the (101) plane of CoOOH (Fig. S2d)[38] SAED also provides evidence for the transformation from amorphous to crystalline (Fig. S2e). At the same time, the content of V and S change greatly compared with that before the test (Fig. S2f). We also analyzed the valence states of Co and V after OER test by XPS (Fig. 4). Notably, the two peaks belonging to Co $2p_{3/2}$ and Co $2p_{1/2}$ move to lower binding energies after the test, mainly because Co^{2+} was oxidized to Co^{3+} during the catalysis (Fig. 4a).[43] In contrast, only V^{3+} is retained in $Co_{0.9}V_{0.1}S_{0.002}$ after the OER because V^{4+} and V^{5+} can be dissolved in an alkaline solution (Fig. 4b).[38] After the OER test, the content of S decreases obviously, and the metal-S bond disappears (Fig. 4c). Based on the above results, we believe that the $Co_{0.9}V_{0.1}S_{0.002}$/NF nanosheets are gradually oxidized to cobalt-vanadium oxide/hydroxide during the OER. The S gradually dissolves during the reaction process to produce S vacancies, and provides more oxidation sites, which causes the amorphous materials to transform into crystalline materials that are more conducive to OER.

Conclusions

In conclusion, we report a method for the synthesis of amorphous $Co_{0.9}V_{0.1}S_{0.002}$/NF nanosheets that catalyze the OER overpotential. When tested for OER performance in 1.0 M KOH solution, this $Co_{0.9}V_{0.1}S_{0.002}$/NF material exhibits optimal catalytic activity, with an overpotential of only 194 mV at a current density of 20 mA cm^{-2} and a Tafel slope of 28.4 mV dec^{-1}. We also measured the long-term electrochemical durability of $Co_{0.9}V_{0.1}S_{0.002}$/NF and found that $Co_{0.9}V_{0.1}S_{0.002}$ is stable for at least 100 h at a current density of 20 mA cm^{-2}. This study not only helps us to understand the active sites and reaction mechanism of MOFs derivatives in OER, but it also provides researchers with a general approach for the design and optimization of MOF based electrocatalysts.

Acknowledgments

This work was supported by the National Natural Science Foundation of China (22074080, 22064010, 51862014, 21775089), Changjiang Scholar Program of the Ministry of Education of China (Q2019258), Taishan scholar of Shandong Province (tsqn201909106), the Natural Science Foundation of Jiangxi Province (20202ACBL213009 and 20212BAB203019).

ORCID

Limin Lu https://orcid.org/0000-0002-3373-695X

References

1. J. Chen, C. Lin, M. Zhang, T. Jin, and Y. Qian, *Chem.Electro.Chem.*, **7**, 3311 (2020).
2. S. Chen et al., *Int. J. Hydrogen Energy*, **46**, 7037 (2021).
3. M. Zhu, Q. Shao, Y. C. Pi, J. Guo, B. Huang, Y. Qian, and X. Huang, *Small.*, **13**, 1701295 (2017).
4. S. Xu, X. Gao, A. Deshmukh, J. Zhou, N. Chen, W. Peng, and H. Gou, *J. Mater. Chem. A*, **8**, 2001 (2020).
5. T. Zhu, J. Ding, Q. Shao, Y. Qian, and X. Huang, *ChemCatChem*, **11**, 689 (2019).
6. H. Chen, Z. Yu, R. Jiang, J. Huang, Y. Hou, Y. Zhang, and W. Tang, *Nanoscale*, **13**, 6644 (2021).
7. Q. Zhang, N. M. Bedford, J. Pan, X. Lu, and R. Amal, *Adv. Energy Mater.*, **9**, 1901312 (2019).
8. R. Bose, V. R. Jothi, K. Karuppasamy, A. Alfantazi, and S. C. Yi, *J. Mate. Chem. A.*, **8**, 13795 (2020).
9. J. Tian, Q. Liu, A. M. Asiri, and X. Sun, *J. Am. Chem. Soc.*, **136**, 7587 (2014).
10. J. Suntivich, K. J. May, H. A. Gasteiger, J. B. Goodenough, and Y. Shao-Horn, *Science*, **334**, 1383 (2011).
11. M. H. Xiang, C. Lu, L. Xia, W. Zhang, J. H. Jiang, F. Qu, and L. Lu, "Catal." *Sci. Technol.*, **10**, 4509 (2020).
12. C. Lu, X. Niu, W. Zhang, F. Qu, and L. Lu, *Sustain. Energy Fuels*, **4**, 5498 (2020).
13. H. Du, X. Zhang, Q. Tan, R. Kong, and F. Qu, *Chem. Commun.*, **53**, 12012 (2017).
14. X. Guo, R. Kong, X. Zhang, H. Du, and F. Qu, *ACS Catal.*, **8**, 651 (2018).
15. L. W. Chen and H. W. Liang, *Catal. Sci. Technol.*, **11**, 4673 (2021).
16. C. Tang, N. Cheng, Z. Pu, W. Xing, and X. Sun, *Angew. Chem. Int. Ed.*, **127**, 9483 (2015).
17. Y. Lee, J. Suntivich, K. J. May, E. E. Perry, and Y. Shao-Horn, *J. Phys. Chem. Lett.*, **3**, 399 (2012).
18. X. Lu and C. Zhao, *Nat. Commun.*, **6**, 6616 (2015).
19. Q. Yang, Q. Xu, and H. Jiang, *Chem. Soc. Rev.*, **46**, 4774 (2017).
20. C. Wu and M. Zhao, *Adv, Mater.*, **29**, 1605446 (2017).
21. Y. B. Huang, J. Liang, X. S. Wang, and R. Cao, *Chem. Soc. Rev.*, **46**, 126 (2017).
22. S. Ji, Y. Chen, S. Zhao, W. Chen, L. Shi, Y. Wang, and Y. Li, *Angew. Chem. Int. Ed.*, **58**, 4271 (2019).
23. E. M. Miner, T. Fukushima, D. Sheberla, L. Sun, Y. Surendranath, and M. Dincă, *Nat. Commun.*, **7**, 10942 (2016).
24. N. Kornienko, Y. Zhao, C. S. Kley, C. Zhu, D. Kim, S. Linand, and P. Yang, *J. Am. Chem. Soc.*, **137**, 14129 (2015).
25. S. Zhao, Y. Wang, J. Dong, C. He, H. Yin, P. An, and Z. Tang, *Nat. Energy*, **1**, 1 (2016).
26. F. L. Li, Q. Shao, X. Q. Huang, and J. P. Lang, *Angew. Chem. Int. Ed.*, **57**, 1888 (2018).
27. X. Lu, P. Liao, J. Wang, J. Wu, X. Chen, C. He, and X. Chen, *J. Am. Chem. Soc.*, **138**, 8336 (2016).
28. W. Cheng, X. Zhao, H. Su, F. Tang, W. Che, H. Zhang, and Q. Liu, *Nat. Energy*, **4**, 115 (2019).
29. C. Z. Yuan, Z. T. Sun, Y. F. Jiang, Z. K. Yang, N. Jiang, Z. W. Zhao, U. Y. Qazi, W. H. Zhang, and A. W. Xu, *Small.*, **13**, 1604161 (2017).
30. Y. Ang, K. Zhang, H. Lin, X. Li, H. C Chan, L. Yang, and Q. Gao, *ACS Catal.*, **7**, 2357 (2017).
31. C. Yang, M. Y. Gao, Q. B. Zhang, J. R. Zeng, X. T. Li, and A. P. Abbott, *Nano. Energy*, **36**, 85 (2017).
32. Y. Wu, Y. Liu, G. D. Li, X. Zou, X. Lian, D. Wang, L. Sun, T. Asefa, and X. Zou, *Nano. Energy.*, **35**, 161 (2017).
33. Q. Yang, Y. Liu, L. Xiao, M. Yan, H. Bai, F. Zhu, and W. Shi, *Chem. Eng. J.*, **21**, 716 (2018).
34. L. Zhang, X. Wang, A. Li, X. Zheng, L. Peng, J. Huang, and Z. Wei, *J. Mate. Chem. A.*, **7**, 17529 (2019).
35. J. Yang, C. Zheng, P. Xiong, Y. Li, and M. Wei, *J. Mate. Chem. A.*, **2**, 19005 (2014).
36. W. Hu, Y. Shi, Y. Zhou, C. Wang, M. R. Younis, J. Pang, and X. Xia, *J. Mater. Chem. A*, **7**, 10601 (2019).
37. W. Li, S. Xue, S. Watzele, S. Hou, J. Fichtner, A. L. Semrau, and R. A. Fischer, *Angew. Chem. Int. Ed.*, **132**, 5837 (2020).
38. Y. Cui, Y. Xue, R. Zhang, J. Zhang, X. Li, and X. Zhu, *J. Mater. Chem. A, 2019.*, **7**, 21911 (2019).
39. K. Fan, Y. Ji, H. Zou, J. Zhang, B. Zhu, H. Chen, Q. Daniel, Y. Luo, J. Yu, and L. Sun, *Angew. Chem. Int. Ed.*, **56**, 3289 (2017).
40. Y. Cui, Y. Xue, R. Zhang, J. Zhang, X. A. Li, and X. Zhu, *J. Mater. Chem. A*, **7**, 21911 (2019).
41. M. Kuang, J. Zhang, D. Liu, H. Tan, K. N. Dinh, L. Yang, and Q. Yan, *Adv. Energy Mater.*, **10**, 2002215 (2020).
42. B. Wang, K. Zhao, Z. Yu, C. Sun, Z. Wang, N. Feng, and Y. Xia, *Energy Environ. Sci.*, **13**, 2200 (2020).
43. H. Xu, K. Ye, K. Zhu, J. Yin, J. Yan, G. Wang, and D. Cao, *Inorg. Chem.Front.*, **7**, 2602 (2020).
44. P. Mohan, J. Yang, A. Jena, and H. S. Shin, *J. Solid State Chem.*, **224**, 82 (2015).
45. H. F. Fan, J. Huang, G. L. Chen, W. Chen, R. Zhang, and K. K. Ostrikov, *ACS. Sustainable. Chem. Eng.*, **7**, 1622 (2019).
46. W. Zeng, G. Zhang, X. Wu, K. Zhang, H. Zhang, S. Hou, C. Li, T. Wang, and H. Duan, *J. Mater. Chem. A*, **3**, 24033 (2015).
47. D. Geng, N.-N. Ding, T. S. A. Hor, S. W. Chien, Z. Liu, and Y. Zong, *RSC Adv.*, **5**, 7280 (2015).
48. L. Wan, J. Xiao, F. Xiao, and S. Wang, *ACS Appl. Mater. Interfaces*, **6**, 7735 (2014).
49. A. Pendashteh, J. Palma, M. Anderson, and R. Marcilla, *Appl. Catal. B-Environ.*, **201**, 241 (2017).
50. X. Zhang, W. Sun, H. Du, R. Kong, and F. Qu, *Inorg. Chem. Front.*, **5**, 344 (2018).
51. K. Fan, H. Chen, Y. Ji, H. Huang, P. M. Claesson, Q. Danieland, and L. Sun, *Nat. Commun.*, **7**, 11981 (2016).
52. S. Trasatti, *Electrochim. Acta*, **29**, 1503 (1984).
53. M. Liu, L. Kong, X. Wang, J. He, and X. H. Bu, *Small*, **15**, 1903410 (2019).
54. X. Yao, L. Zhuang, Y. Jia, H. Liu, Z. Li, L. Zhang, and Z. Zhu, *Angew.Chem. Int. Ed.*, **59**, 14664 (2020).
55. X. Yu, Z. Y. Yu, X. L. Zhang, P. Li, B. Sun, X. Gao, and S. H. Yu, *Nano Energy.*, **71**, 104652 (2020).